Astron. Astrophys. 346, 599–603 (1999)

ASTRONOMY AND ASTROPHYSICS

ROSAT HRI observation of the supernova remnant Kes 32 and the nearby radio pulsar PSR B1610−50

W. Brinkmann[1], **N. Kawai**[2], **H. Scheingraber**[1], **K. Tamura**[3], **and W. Becker**[1]

[1] Max-Planck-Institut für Extraterrestrische Physik, Giessenbachstrasse, D-85740 Garching, Germany
[2] Cosmic Radiation Laboratory, RIKEN, 2-1 Hirosawa, Wako-shi, Saitama 351-01, Japan
[3] VBL, Nogoya University, Furo-chu, Chikusa-ku, Nagoya, Japan

Received 10 November 1998 / Accepted 18 February 1999

Abstract. We present the results of a deep ROSAT HRI observation of the supernova remnant Kes 32 and the possibly associated pulsar PSR B1610-50. The supernova remnant shows strongly energy dependent complex structures in a comparison with the ASCA GIS and ROSAT PSPC data with low foreground absorption ($N_H \sim 5 \times 10^{21}$ cm^{-2}). The pulsar is not seen in the HRI image indicating a high absorbing column density ($N_H \gtrsim 5 \times 10^{22}$ cm^{-2}) along the line of sight, making the physical connection between Kes 32 and *PSR B1610−50*unlikely. The elongated structure south of the pulsar, interpreted as a pulsar jet, might be an unrelated foreground emission.

Key words: ISM: supernova remnants – ISM: jets and outflows – stars: pulsars: individual: PSR B1610-50 – X-rays: ISM

1. Introduction

Kes 32 (G332.4+0.1, MSH 16-51) is a supernova remnant (SNR) with a peculiar morphology (Kesteven 1968, Roger et al. 1985). It has a size of approximately 15′ and a flux density at 1 GHz of 26 Jy. While its main body is a fairly typical shell-type radio SNR, a jet-like feature seems to emerge from it on the north-east and to expand into an extended dim plume. The shell is brightest at the north-west rim and the south-east rim, corresponding to the sides of lowest and highest galactic latitudes. Despite their remarkable association, the shell and the jet-like feature have different emission characteristics. The shell has a non-thermal spectrum with a power law $\alpha_r \sim -0.45$–0.55 and is partially linearly polarized. The outflow structure, on the other hand, has a flat spectral index (-0.05) and no polarization could be detected. Recent MOST observations at 843 MHz and a comparison with 60 μm IRAS images shows that both the jet and plume are likely to be thermal and probably unrelated to the remnant (Whiteoak & Green 1996).

The remnant contains a point radio source approximately at the center of the shell, but no radio pulsations have been detected from it. The distance to Kes 32 is highly uncertain. The distance of $\sim$ 3.3 kpc to RCW 103, a supernova remnant 30 arcmin away with soft X-ray emission, is referred to as the lower limit for the distance to Kes 32. An upper limit of $\sim$7 kpc is derived from a weak OH absorption and from the $\Sigma - D$ - relation. If an (arbitrary) intermediate distance of 5 kpc is adopted, the diameter of the SNR is $\sim$25 pc, and the age expected from the standard Sedov relation is $\sim$ 5000 yr (Roger et al. 1985).

Recently, it has been proposed that Kes 32 is associated with the radio pulsar PSR B1610−50 (Caraveo 1993) which is located outside the radio shell at an angular distance of $\sim 10'$ from the shell center. The distance to the pulsar is also uncertain, being anywhere between 5 kpc and 15 kpc (Taylor et al. 1993). With its characteristic age of 7450 yr, it is the 4th youngest among the known pulsars next to PSR B0540−69 in the LMC ($T_c = 1670$ yr), and it is younger than the Vela pulsar ($T_c = 11350$ yr). If the pulsar was born at the center of Kes 32, the derived velocity of the pulsar is at least 1600 km s^{-1} for the assumed distance of 5 kpc. If this is indeed an example of a high velocity pulsar, it can be evidence to support the newly proposed distribution of the pulsar velocities (Lyne & Lorimer 1995) which predicts some pulsars with velocities $>$ 1500 km s^{-1}. Since the pulsar is located opposite to the jet-like plume, it has been argued that it could be carrying part of the momentum of the progenitor, which may have generated the plume as a result of the interaction with the ambient material before it arrived the site of the supernova, i.e. the center of Kes 32 (Caraveo 1993).

In X-rays Kes 32 was observed by the Einstein observatory, but no significant flux was detected (Lamb & Marker 1981). The region containing Kes 32 was in the field of view of a 30 ksec ROSAT PSPC (Position Sensitive Proportional Counter) observation of RCW 103. A broad diffuse emission was found to extend from RCW 103 towards Kes 32, but the X-ray structure of Kes 32 can not be studied in detail as the object falls directly on the inner support structure of the PSPC detector.

The field containing PSR B1610−50 and Kes 32 was observed with ASCA (Tanaka et al. 1994) on March 25, 1994 for a total exposure of about 22 ksec. As the observation was focused on PSR B1610−50, only a part of the west shell of Kes 32 was in the field of view. The Gas Imaging Spectrometer (GIS) captured the main body (shell) of Kes 32, but the 'plume' of Kes 32 is mostly out of the field of view. *PSR B1610−50*, the original

Send offprint requests to: W. Brinkmann (wpb@mpe.mpg.de)

target of the observation was only seen in the GIS image above 2 keV. The radial profile of the source at the position of *PSR B1610−50*is consistent with a point source, but a flat circular distribution with a radius up to ~ 1 arcmin cannot be rejected. Further, there seems to be structure in the GIS image extending $\sim 10'$ to the south of the pulsar. Although its physical association with Kes 32 and the pulsar cannot be confirmed, it was claimed not to be a foreground object because it is absorbed and more clearly visible in the hard band (Kawai & Tamura 1996).

In this paper we will present the analysis of a ~ 50 ksec observation with the ROSAT High Resolution Imager (HRI). The data with superior spatial resolution are compared with results of the ASCA observation, providing high spectral accuracy over a much wider energy band of ∼0.5–8 keV (Kawai & Tamura, in prep.) and, where possible, with the PSPC data. In Sect. 2 we will first discuss the spatial structure of the system derived from the ROSAT observation. Then, we will present a comparison of the data with the ASCA results.

2. The X-ray observation

The field containing PSR B1610−50 and Kes 32 was observed with ROSAT HRI for ~ 52 ksec in 1997 from March 13, UT 23:51 to March 18, UT 08:37. The detector was pointed at the position of the pulsar and a total of ~ 265.000 photons were collected. However, due to the proximity of the objects close to the Galactic plane and the long observation most of the detected photons must be attributed to external and detector background emission.

In Fig. 1 we show the HRI brightness distribution overlayed with the X-ray contours obtained from the ASCA GIS detector in the hard ≥ 2.2 keV energy range. The HRI data were binned into $30'' \times 30''$ pixels and additionally smoothed with a Gaussian 15×15 pixel filter with a sigma of 3 pixels. The color bar for the intensity scale is given at the bottom; the left, dark blue color corresponds to 52 counts/pixel, the white color at the right corresponds to the maximum of ~ 58.6 cts/pixel. The GIS contour lines are in multiples $0.057 \times$ the peak value in the image. The encircled cross in the center indicates the position of the pulsar.

It must be noted that in the ASCA band the geometrical appearance of the emission is highly energy dependent. Further, due to the complex point spread function of the ASCA XRT and due to the limited photon statistics in both instruments small-scale details of the spatial structures must be taken with care as they are particularly affected by the applied smoothing of the data.

There appears to be a complex correlation on larger scales between the pattern in the hard and very soft energy band. However, the two most obvious structures are anti-correlated: the brightest spot in the ASCA band on the north rim of Kes 32 coincides with an extended minimum in the soft HRI band. And the flux maximum on the pulsar falls directly onto an emission hole of the HRI image. In this connection it is worth to notice, that even in the $E \leq 2.2$ keV GIS band the pulsar is not seen.

2.1. Is the signal real?

As mentioned above, most of the detected photons must be attributed to various kinds of external background emission and instrumental background. Therefore a more detailed assessment of the signal - to - noise seems to be appropriate to ensure the physical reality of the observed structures. In fact, the average number of counts over the HRI field of view was $< N_{obs} >= 14.1 \pm 4.3$ per $15'' \times 15''$ pixel, the average number of expected total HRI background counts in a $\lesssim 52$ksec observation in that pixel size is 12.35 (Briel et al. 1997). We tested the distribution of the counts/pixel and found that this distribution is neither consistent with pure background fluctuations nor with a superposition a Poissonian background plus a random signal.

Some of the structures are seen in the two completely independent instruments, the ROSAT HRI as well as the ASCA GIS which gives further confidence in the reality of these structures. However, the images show considerable energy dependences and both are of similarly low statistical significance.

Finally, the left hand side of Fig. 1 is seen relatively undisturbed in the above mentioned PSPC image while the right half is heavily obscured by the PSPC's support structure. The intensity distribution in the undisturbed part of the PSPC image matches very well the features seen in the HRI.

These findings provide strong confidence in the physical reality of the structures. To obtain a more quantitative measure we analyzed the HRI image with an advanced spatial filtering method, developed to filter a signal out of background noise, based on the usage of scaling indices. For every photon (point) in the two-dimensional image a scalar quantity, the so called scaling index α is determined. α is a measure for the local fractal dimension in the neighborhood of the point (Halsey et al. 1986). The spectrum of all these indices, $f(\alpha)$, is a sensitive tool for the correlation analysis of a point set or an image (Ebeling & Wiedenmann 1993, Wiedenmann et al. 1998). In the limit of an infinitely extended, two dimensional homogeneous and random point set, e.g., white noise, $f(\alpha)$ approaches a delta function at $\alpha = 2$. Spectral structures at values larger than $\alpha \gtrsim 2$ are indicators for boundary effects, features at $\alpha \lesssim 2$ indicate substructures in the image.

The upper panel of Fig. 2 shows as dotted line the scaling index spectrum for the spatially randomized photons of the HRI observation (surrogate data). The integral of the curve equals the total number of photons in the image ~ 265000 and it approaches that of pure white noise with a weak high-α tail originating from the finite size of the image. The peak value of the normalized random distribution corresponds to ~ 30000 photons for the binning of $\Delta\alpha = 0.01$ used in Fig. 2. The full line represents the spectral distribution of the observed photons showing clearly strong deviations from pure noise on smaller spatial scales. To further demonstrate the reality of the signal we plot in the lower panel of Fig. 2 as dotted line the integrated differences of two different sets of surrogate data to demonstrate the magnitude of statistical fluctuations. The full line describes the difference between the actual data and a random distribution, which corresponds to the photons in the signal. This clearly

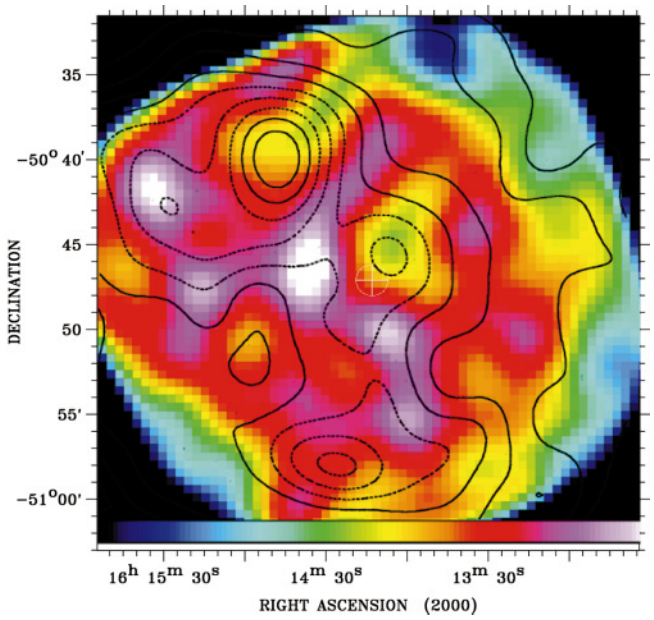

Fig. 1. Overlay of GIS contour lines ($E \geq 2.2$ keV) onto the smoothed ROSAT HRI brightness distribution.

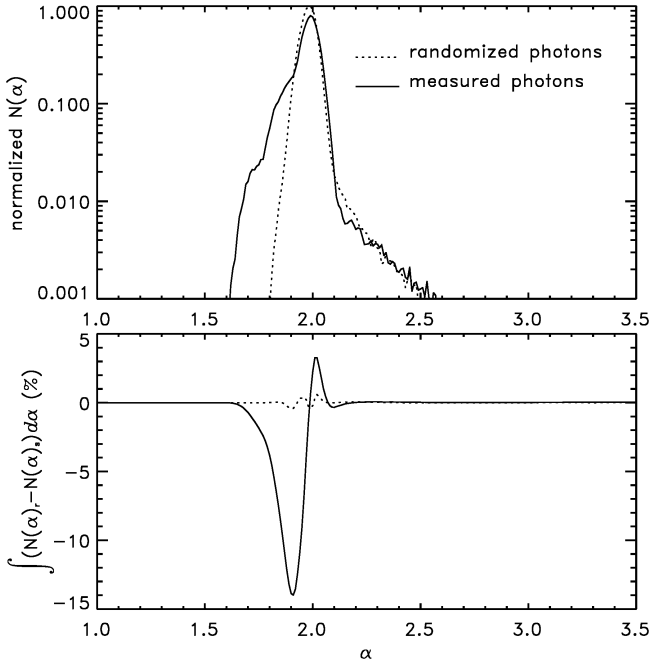

Fig. 2. Distribution of scaling indices from the HRI data (full lines) and surrogate data. *Top:* normalized spectra; *bottom:* differences between surrogate data and measured photons (see text).

shows that the structures in Fig. 1 result from a signal which is far above any statistical fluctuation.

2.2. Kes 32

In Fig. 3 (top panel) we present an overlay of the 843 MHz MOST radio contours (Whiteoak & Green 1996) with that part of the HRI image spatially covering the supernova remnant, i.e.

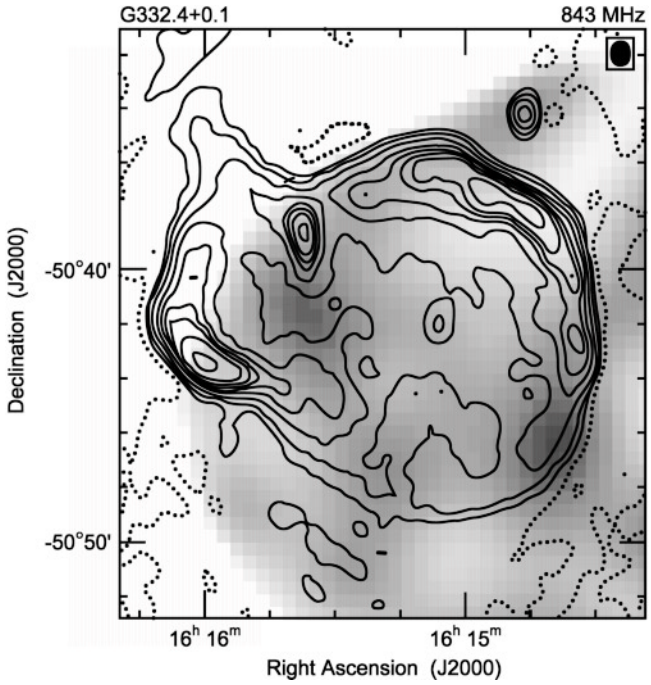

Fig. 3. Radio contour lines of Kes 32 overlayed on the HRI brightness distribution

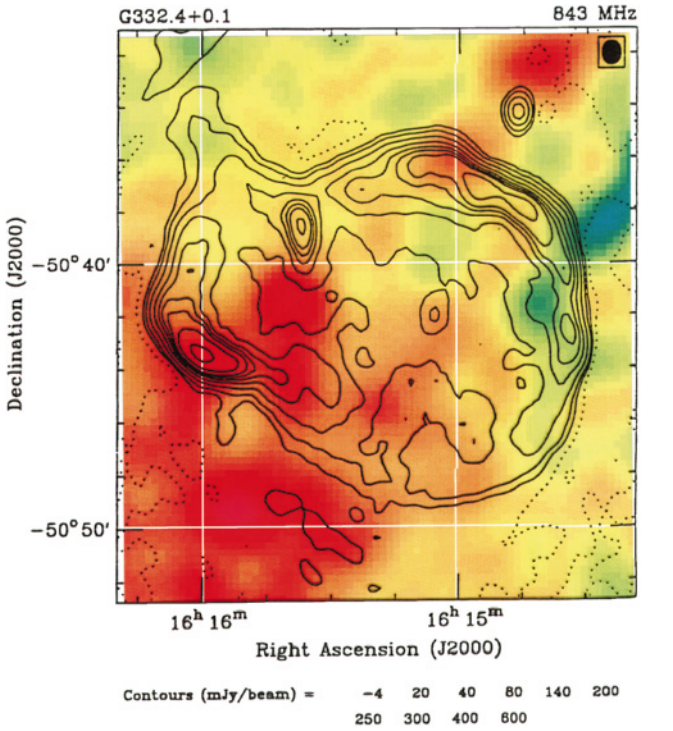

Fig. 4. Radio contour lines of Kes 32 overlayed on the smoothed PSPC brightness distribution. Note, that the right half of the image is heavily (non-uniformly) under-exposed due to the wobbling motion of the detectors support structure.

the gray shaded region. Interestingly, the bright X-ray emission in the east is at the position of the radio outbreak of the plume, the elongated emission in the south occurs in regions

of low radio surface brightness as well and only the western brighter X-ray structure coincides with the rim of the remnant. The north-eastern radio rim of Kes 32 is a region of enhanced X-ray emission as well, however this is very close to the edge of the HRI detector. The radio bright north-western boundary of the SNR is coincident with a region of very low soft X-ray flux.

A similar pattern can be seen in the image obtained from the PSPC observation (Fig. 4; with color coding analogous to that of Fig. 1) where we find additionally a very luminous X-ray structure directly on the bright radio feature in the south-east which is outside the HRI's field of view. The north-eastern region of the image outside the HRI field of view appears flat and structureless in the PSPC. Unfortunately, the PSPC's ring support structure runs approximately diagonally (top middle to right bottom) across the image as well as one of the radial spokes to the upper right (the blue intensity minima). The PSPC's wobbling motion with an amplitude of $6'$ obscures then heavily part of the remnant, clearly recognizable from the lighter greenish - blue color, and thus the south-western region of the image does not provide any useful information.

The bright northern emission in the ASCA image has been interpreted as thermal emission from a gas in ionizational non-equilibrium with temperature around $kT \gtrsim 4$ keV and a small relaxation parameter implying a young age of the remnant. The spectrum in the Solid state Imaging Spectrometer (SIS) clearly shows strong Si, S, and Ar line emission on a relatively hard continuum but the exact form of the spectrum remains uncertain due to the limited photon statistics (Kawai & Tamura 1996).

The ROSAT HRI and PSPC detectors both exhibit pronounced emission holes at the position of the GIS maximum (see Fig. 1). The SIS spectrum does not indicate abnormally high absorption. The fitted values are around $N_H \sim 5 \times 10^{21}$ cm^{-2} which is insufficient to 'hide' this emission in the softer ROSAT band. We must therefore conclude that the emission from the remnant in that region is more likely distributed along the rim, with a central emission minimum. However, the different spectral responses as well as the limited photon statistics in the lower resolution ASCA images might contribute as well to the partly contrasting appearance of the two images.

2.3. The pulsar

As a Vela-type pulsar (Becker & Trümper 1997) *PSR B1610−50* is expected to exhibit strong steady emission from a pulsar-powered synchrotron nebula with a small pulsed contribution of magnetospheric or thermal origin. However, apart from the Vela pulsar itself there is no spectral information for these sources at low energies as they are distant and suffer from photoelectric absorption.

The ASCA GIS spectrum of the pulsar can be quite well fitted with a single power law. However, there is clearly low energy source confusion from the surrounding region: a fit of the data over the total GIS energy range yields a power law photon index of $\Gamma \sim 1.5$ with an absorbing column density of $N_H = 1.2 \times 10^{22}$ cm^{-2}. Restricting the photons to the energy range $E > 2$ keV, we obtain a photon index $\Gamma = 2.0$ and an $N_H = 3.4 \times 10^{21}$ cm^{-2}. In both cases the normalizations are similar, $N_o = 7.1 \times 10^{-4}$ and $N_o = 9.7 \times 10^{-4}$ photons cm$^{-2}s^{-1}$ at 1 keV, respectively.

The pulsar is not visible in the soft ROSAT HRI band. This must be caused by strong absorption which cannot be determined accurately from the ASCA data due to the source confusion. Taking the HRI 1 σ error of ~ 4.3 counts as an upper limit to the pulsar emission during the HRI observation and the slopes and normalizations of the above two power law fits, N_H values of $\gtrsim 7.2 \times 10^{22}$ cm^{-2} are required in both cases to render the pulsar undetectable (1σ) in the HRI band in a ~ 52 ksec observation.

This value is slightly larger than the Galactic absorption column density $N_{H\ Gal}$ of $\sim 2.5 \times 10^{22}$ cm^{-2} obtained from HI surveys in this direction (Dickey & Lockman 1990).

The pulsar's dispersion measure of DM = 586 $\pm$ 5 predicts a distance of 7.3 kpc, employing the Galactic electron density distribution model of Taylor & Cordes (1993). This model yields distances which are on average correct up to a nominal error of about 25%. The inferred average electron number density is of the order of ~ 0.08 cm^{-3}. Taking the 'standard' relation between the numbers of free electrons per hydrogen atom $\sim$0.1, we obtain an estimate for the hydrogen column density of $\sim 1.8 \times 10^{22}$ cm^{-2} towards the pulsar.

The values for the amount of material along the line of sight, i.e., the particle number densities and/or the distances, obtained from either the X-ray or the radio measurements are thus slightly different but consistent inside their mutual errors, in particular, if the systematic uncertainties of the X-ray spectral fits are considered.

Both measurements seem to imply rather large distances to the pulsar, far in excess of the estimated distance of Kes 32.

The emission south of the pulsar detected in the hard band GIS image remains visible in the HRI image as well, but not as a clear, southwards pointing connected structure which led to the interpretation as a 'pulsar jet' (Kawai & Tamura 1996). This implies that the foreground absorption column density is much lower which indicates that this emission is not causally connected to *PSR B1610−50*. Unfortunately, the intrinsic spectral shape of the structure is poorly known and the region might be heavily contaminated by soft foreground emission.

3. Conclusions

The spatial region around the SNR Kes 32 and the pulsar *PSR B1610−50*was observed with ASCA, the ROSAT PSPC and the HRI. Due to various instrumental limitations and, generally, too low signal - to - noise ratios no definite physical picture can be obtained from these X-ray observations.

It appears that the X-ray structure of the SNR is rather complex. There are spatial regions where X-ray and radio emission are strongly correlated, at the north-eastern and the south-western rim (see Fig. 3) and in the south-eastern knot visible only in the PSPC image (Fig. 4). This indicates a common origin of the radiation at both wavelengths, i.e, from the remnant's

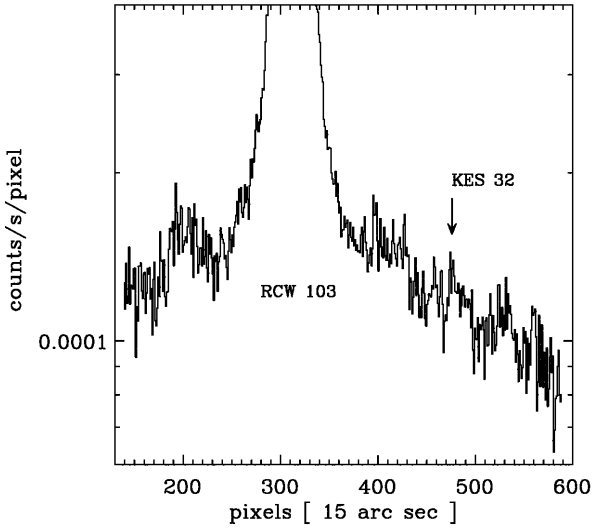

Fig. 5. Exposure corrected intensity profile of the PSPC observation from a $\sim 12'$ wide strip from Kes 32 towards RCW 103 and beyond.

shock front. The region, extending from the central point-like radio structure to the bright north-western rim and beyond is devoid of X-ray emission.

Interestingly, two strong local X-ray maxima are located in regions of minimal radio flux: in the very south and at the base of the jet-like feature opening further out into the plume. The physical reason for this anti-correlation remains unknown. However, as this X-ray emission occurs in regions where the form of the remnant clearly deviates from a circular shape, and as there are claims that the jet structure and the plume are unrelated to the remnant (Whiteoak & Green 1996) it appears plausible that we are seeing the spatial superposition of otherwise unrelated sources in X-rays as well. This question can only be solved by future deeper imaging X-ray missions in the higher energy band.

However, any study of this remnant will be affected by the extended X-ray emission found over large scales around the nearby SNR RCW 103. Its angular size of a few degrees, as visible in the All Sky Survey, indicates that it is foreground emission.

Fig. 5 shows an intensity profile over the $\sim 2^o$ of the PSPC detector, taken from Kes 32 southwards across RCW 103. Plotted is the averaged exposure corrected count rate in a $15'' \times 15''$ pixel. Visible in the center is the very dominant emission from RCW 103. Part of the fluctuations come from individual point sources in the field of view. The Galactic plane cuts the profile (obliquely) near the pixels 410; the strong emission at pixels 520–550 is the soft Einstein source 2E 1611.1-5018, very likely coincident with the 10^{th} magnitude G5 star CD-50 10271. The whole X-ray bright region south of RCW 103 is spatially coincident with a large molecular cloud of the Gould belt (Bronfman et al. 1989) containing as well dense dark clouds (Feitzinger & Stüwe 1984). Although the majority of this emission is located south of RCW 103 and Kes 32 is located at the northern, fading rim of the extended X-ray flux it cannot be ruled out that part of the structures found in the images above are chance coincidence superpositions of emission unrelated to Kes 32.

Similar reservations must hold for the X-ray structures south of the pulsar. The fact that the pulsar is not seen in the HRI's soft band pass indicates strong absorption towards the object and thus a large distance. Therefore, the emission from the putative 'pulsar jet' (Kawai & Tamura 1996) appears to be unrelated foreground emission, although the largely uncertain spectral properties of might influence the appearance of these structures in the different energy bands.

Only future observations with imaging instruments which combine good spatial resolution with spectral capabilities at harder X-rays will unambiguously solve this puzzle.

Acknowledgements. The ROSAT project is supported by the Bundesministerium für Bildung, Wissenschaft, Forschung und Technologie (BMBF) and the Max-Planck-Gesellschaft. WB & WB thank the Cosmic Radiation Laboratory for hospitality where part of the research was done in the framework of the RIKEN - MPG exchange program.

References

Becker W., Trümper J., 1997, A&A 326, 682
Briel U.G., Aschenbach B., Englhauser J., et al., 1997, ROSAT User's Handbook, $http://www.xray.mpe.mpg.de$
Bronfman L., Alvarez H., Cohen R.S., Thaddeus P., 1989, ApJS 71, 481
Caraveo P.A., 1993, ApJ 415, L111
Dickey J.M., Lockman F.J., 1990, ARA&A 28, 215
Ebeling H., Wiedenmann G., 1993, Phys. Rev. E 47, 704
Feitzinger J.V., Stüwe J.A., 1984, A&AS 58, 365
Halsey T.C., Jensen M.H., Kadanoff L.P., Rocaccia I., Shraiman B.I., 1986, Phys. Rev. A 33, 1141
Kawai N., Tamura K., 1996, In: Johnston S., Walker M.A., Bailes M. (eds.) Proc. IAU Colloquium 160, ASP Conf. Series, San Francisco, p. 367
Kesteven M.J.L., 1968, Aust. J. Phys. 21, 369
Lamb R.C., Marker T.H., 1981, ApJ 244, 94
Lyne A.G., Lorimer D.R., 1995, JApA 16, 97L
Roger R.S., Milne D.K., Kesteven M.J., Haynes R.F., Wellington K.J., 1985, Nat 316, 44
Tanaka Y., Inoue H., Holt S.S., 1994, PASJ 46, L37
Taylor J.H., Cordes J.M., 1993, ApJ 411, 674
Taylor J.H., Manchester R.N., Lyne A.G., 1993, ApJS 88, 529
Whiteoak J.B.Z., Green A.J., 1996, A&AS 118, 329
Wiedenmann G., Scheingraber H., Voges W., 1998, In: diGesu V., et al. (eds.) Data Analysis in Astronomy V, World Scientific, Singapore, in press